Similarities and differences of face and body perception in the dog (*Canis familiaris*) and human brain

Magdalena Boch[1,2*], Isabella C. Wagner[1], Sabrina Karl[3], Ludwig Huber[3+] and Claus Lamm[1,4+]

[1]Social, Cognitive and Affective Neuroscience (SCAN) Unit, Department of Cognition, Emotion, and Methods in Psychology, Faculty of Psychology, University of Vienna, Vienna, Austria

[2]Department of Cognitive Biology, Faculty of Life Sciences, University of Vienna, Vienna, Austria

[3]Comparative Cognition, Messerli Research Institute, University of Veterinary Medicine Vienna, Medical University of Vienna and University of Vienna, Vienna, Austria

[4]Vienna Cognitive Science Hub, University of Vienna, Austria

[+]These authors share senior authorship.

*Corresponding author:

Email: magdalena.boch@univie.ac.at

Abstract

Accurately recognizing other individuals is fundamental for successful social interactions. While the neural underpinnings of this skill have been studied extensively in humans, less is known about the evolutionary origins of the brain areas specialized for recognising faces or bodies. Studying dogs (*Canis familiaris*), a non-primate species with the ability to perceive faces and bodies similarly to humans, promises insights into how visuo-social perception has evolved in mammals. We investigated the neural correlates of face and body perception in dogs (N = 15) and humans (N = 40) using functional MRI. Combining uni- and multivariate analysis approaches, we identified activation levels and patterns that suggested potentially homologous occipito-temporal brain regions in both species responding to faces and bodies compared to inanimate objects. Crucially, only human brain regions showed activation differences between faces and bodies and partly responded more strongly to humans compared to dogs. Moreover, only dogs represented both faces and dog bodies in olfactory regions. Overall, our novel findings revealed a prominent role of the occipito-temporal cortex in the perception of animate entities in dogs and humans but suggest a divergent evolution of face and body perception. This may reflect differences in the perceptual systems these species rely on to recognize others.

1 Introduction

The ability to detect and recognize another individual is a socio-cognitive skill crucial for successful social interactions and survival. The face and body of another human or non-human animal convey a wealth of social information beyond their identity, such as when facilitating the correct categorization of another individual's emotional state [1–7]. Consequently, accurate perception of faces and bodies is an important building block for social perception.

Therefore, the neural underpinnings of face and body perception have been studied extensively in humans. Decades of research revealed a predominant role of the occipito-temporal cortex for the perception of others with distinct, but adjacent regions specialized for face and body perception as part of the so-called ventral visual pathway [8–17]. While the ventrolateral visual cortex responds to animate compared to inanimate stimuli more generally [18–20], the sensitivity in the occipital face and extrastriate body area (lateral occipital cortex), as well as the fusiform face and fusiform body area (inferior temporal cortex) appear increased for faces or bodies [10,11,24–28,12,13,15–17,21–23]. Regarding the recognition of another individual's species-identity, previous research suggests a preference for human faces compared to faces of other species (such as dogs or horses) [29,30], potentially reflecting increased salience of conspecifics over heterospecifics.

The evolutionary history of the neural underpinnings of face and body perception has been mainly investigated by comparative research in non-human primates [23–27,31], and this has revealed a homologous visual pathway [e.g., 1 for review]. However, apart from primate species, the neural bases of this socio-cognitive ability and its potential origin in the mammalian brain remain largely unstudied. Dogs' (*Canis familiaris*) ability to perceive and understand humans and conspecifics has already been well-investigated using behavioural and eye-tracking

measures and yielded numerous comparable skills between dogs and humans. For example, dogs can not only differentiate between faces [32,33], but even discriminate facial emotional cues of humans and conspecifics [7,34,35]; and they demonstrate complex behaviours such as visual perspective taking [36,37]. Thus, dogs constitute an excellent model to study the evolution of visuo-social perception in mammals [38].

While first non-invasive canine neuroimaging studies [29,39–42] suggested an involvement of the temporal cortex in face perception, they triggered a debate on whether the occipito-temporal specialization for face perception in dogs matches that of humans [29,39–42]. Previous work reported increased activation for faces compared to objects [40,42], scenes [40], or a mono-coloured surface [39], but not compared to other low-level visual controls (i.e., scrambled images [39,40] or the back of the head [29]). Some studies lacked non-facial controls entirely [41]. Studies additionally investigating responses to con- and heterospecifics were inconclusive ranging from reports of increased responsiveness to dog stimuli in general (i.e., face and back of the head) but no specialization for faces [29], over separate brain regions specialized for human or dog faces [41], to no species- but general face-preference [40]. Further, no previous work investigated the neural bases of body perception. This is a major limitation, as bodies play an important role for social perception in general, but in particular for dogs - as indicated e.g., by dogs' high responsiveness to emotional or ostensive-referential bodily cues, such as tail-wagging [43] or human gestures [43–45]. It is particularly noteworthy in this respect, that dogs even outperform humans' closest living relatives, chimpanzees, in utilizing human ostensive cues [46].

Thus, the findings so far do not allow for a distinction between face and body or general animacy perception and are inconclusive regarding the influence of the other individual's species-identity. The present comparative neuroimaging study aimed to

resolve this debate. We performed the, to our knowledge, first systematic comparison of the neural bases of face, body and inanimate object perception in dogs and humans, in order to gain insights into how social perception has evolved in two phylogenetically distant mammalian species [38,47].

2 Results

Fifteen awake and unrestrained pet dogs (**Fig 1A**) and forty human participants underwent functional magnetic resonance imaging (MRI) while viewing images of human and dog bodies, faces, inanimate objects (e.g., different toys), and grid-scrambled versions of these images serving as visual controls (**Fig 1B**). Over the course of two 5 min runs, participants saw 180 different images presented in a block design interspersed with an implicit visual baseline. We analysed the dog fMRI data with a newly developed analysis protocol shown to significantly improve neural signal detection power [48]. All statistical tests were corrected for multiple comparisons (see **fMRI data analysis**, **Fig 2**, **Tables S2-S3**).

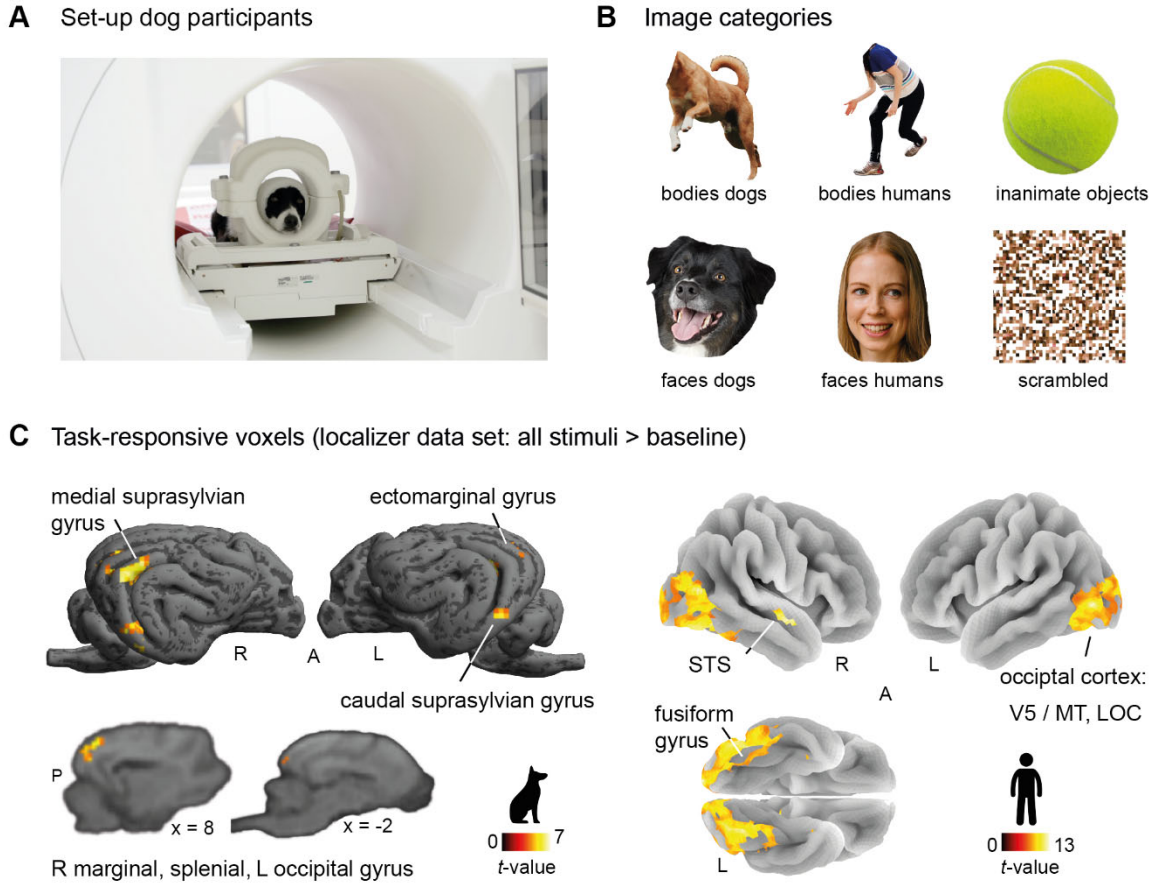

Fig 1. *Overview of the comparative experimental approach to study the neural bases of face and body perception in dogs and humans.* (**A**) We obtained all imaging data using a 3T Siemens Skyra MR-system, equipped with a 15-channel human knee coil to scan the dog participants, and using a 32-channel human head coil for the human participants (not depicted). Dogs received extensive training [49] to stay motionless without restraints or sedation and could leave the MR scanner at any time via a custom-made ramp positioned at the scanner bed. All (dog and human) participants wore earplugs for noise protection and dog participants had an additional head bandage to secure optimal positioning of the earplugs throughout the scan session. (**B**) All participants viewed images of human and dog bodies, human and dog faces, inanimate objects (e.g., toys) or grid-scrambled versions of these images presented in a block design. (**C**) We split the data sets and used data from the first task run to compare activation for visual stimulation (all stimuli) to the visual baseline (i.e., the localizer data set). In both participant samples, we observed activation in the occipito-temporal cortices. These task-responsive voxels then served as a search space to determine individual functional regions-of-interest (fROIs), additionally constrained by bilateral anatomical regions (see **Fig 2A**). Results are displayed at $p < 0.05$, *FWE*-corrected at cluster-level using a cluster-defining threshold of $p < .001$ (dogs, Table S1), and $p < 0.05$ whole-brain *FWE*-corrected (humans; **Table S1**) Results for the dogs are overlaid onto a canine breed-averaged surface render [50], and onto the FreeSurfer "FsAverage" surface for humans (https://surfer.nmr.mgh.harvard.edu/fswiki). Anatomical nomenclature for all figures refers to the dog brain atlas from Czeibert and colleagues [51] and to the human brain atlas from the Laboratory for Neuro Imaging (LONI) Brain Atlas [52] (LPBA40; http://www.loni.usc.edu/atlases/). R, right; L, left; A, anterior; P, posterior; STS, superior temporal sulcus; MT, middle temporal visual area (V5); LOC, lateral occipital complex.

2.1 Mass-univariate analysis: Face- or body-sensitive areas in the occipito-temporal cortices of dogs and humans

To start out, we investigated whether dogs and humans have specialized cortical regions for face and body perception, and whether these regions responded differently to images of con- or heterospecifics. To this end, we used a standard functional region-of-interest analysis approach (fROI,[53–55]). We split the data into two orthogonal data sets, (1) a localizer data set (first task run) to define potential face- or body-sensitive

areas in visual-responsive brain regions (**Fig 1C, 2A**) and (2) a test data set (second task run) to extract activation levels from these regions and to test potential category sensitivity. We chose this approach for two reasons. First, we aimed at directly testing the potential category-sensitivity, quantified by increased activation levels. Second, our goal was to account for differences in the location of activation peaks between individuals as reported in previous dog imaging studies [40,42].

2.1.1 Functional regions-of-interest (fROIs)

For each participant, we defined bilateral fROIs within constrained search spaces to preserve spatial information (i.e., the rough anatomical location of activation peaks). For the human participants, we used previously reported anatomical regions known to be engaged in face and body perception [56]: the extrastriate body area, fusiform body area, occipital face area and fusiform face area (**Fig 2A**). For the dog participants, we could not build on previous research due to lack of shared template space and availability of data. Therefore, we first compared activation levels associated with the visual presentation of all stimuli compared to implicit baseline (i.e., white cross presented on grey background) using the localizer data set. This revealed task-responsive activation within the occipital-, splenial-, ectomarginal-, caudal-, medial suprasylvian- and marginal gyri, partially overlapping with results from previous studies investigating face perception [29,39–42,57,58] (**Fig 1C**, **Table S1**). We then used anatomical masks [51] of these regions as search spaces for the dog participants (**Fig 2A**). For comparison, we also report task-responsive voxels for the human participants, confirming involvement of the occipito-temporal cortex including the lateral occipital cortex and fusiform gyrus (**Fig 1C**, **Table S1**; see also **Fig. S1** for schematic figures of the dog and human brain).

We then defined individual category-sensitive regions within each search space by selecting the top-10% voxels with the strongest activation for bodies or faces compared to inanimate objects based on the individual data from each participant.

2.1.2 Sensitivity for animate stimuli but sub-division in face- and body-sensitive regions exclusive to humans

Next, we extracted the mean activation signal during viewing of faces, bodies, inanimate objects and scrambled images (all compared to the implicit baseline) from the individual fROIs using the test data set. In dogs, we observed significantly increased activation levels for faces and bodies compared to inanimate objects or scrambled images in both face and body fROIs, located in the medial and caudal suprasylvian- and ectomarginal gyrus. In the caudal suprasylvian face- and ectomarginal body fROI, the increased activation for faces showed the same trend but did not always reach significance. We did not find consistent evidence for a further sub-division into face- and body-selective areas in the occipito-temporal cortex, as there was no significant activation difference between faces and bodies in seven out of eight fROIs. We only observed significantly increased activation for bodies compared to faces in the caudal suprasylvian face but not body fROI. The occipital and splenial face and body fROIs did not result in differential activation changes in response to any of the stimulus categories (**Table S2**). Regarding the parietal cortex, the marginal gyrus appeared solely responsive to bodies compared to all other conditions with no activation differences for faces compared to inanimate objects or scrambled controls (**Fig 2B**).

Results for the human participants confirmed earlier research [10,11,24–28,12,13,15–17,21–23] with the strongest overall activation levels for bodies in the extrastriate and fusiform body areas and for faces in the occipital and fusiform face areas (**Fig 2B**; **Table S2**). In summary, we found multiple occipito-temporal regions in

the dog and human cortices responsive to animate stimuli, but detected a further sub-division into face- and body-sensitive regions exclusively in the human brain (see also **Fig S1** for a summary of the results).

2.1.3 Conspecifics preference in human extrastriate body and fusiform face area

Next, we investigated whether processing of faces or bodies differed when participants saw images of con- compared to heterospecifics (**Table S3**). In humans, this revealed increased activation for human (mean: 4.46, *SD* = 1.83) compared to dog bodies (mean: 3.76, *SD* = 1.66) in the extrastriate body area ($t(39) = 3.14$, $p = 0.003$), as well as a general activation increase for human (mean: 1.89, *SD* = 0.87) compared to dog (mean: 1.64, *SD* = 0.81) stimuli in the fusiform face area ($t(79) = 3.71$, $p < 0.0001$). For the dogs, we did not find a difference between the perception of dog and human stimuli.

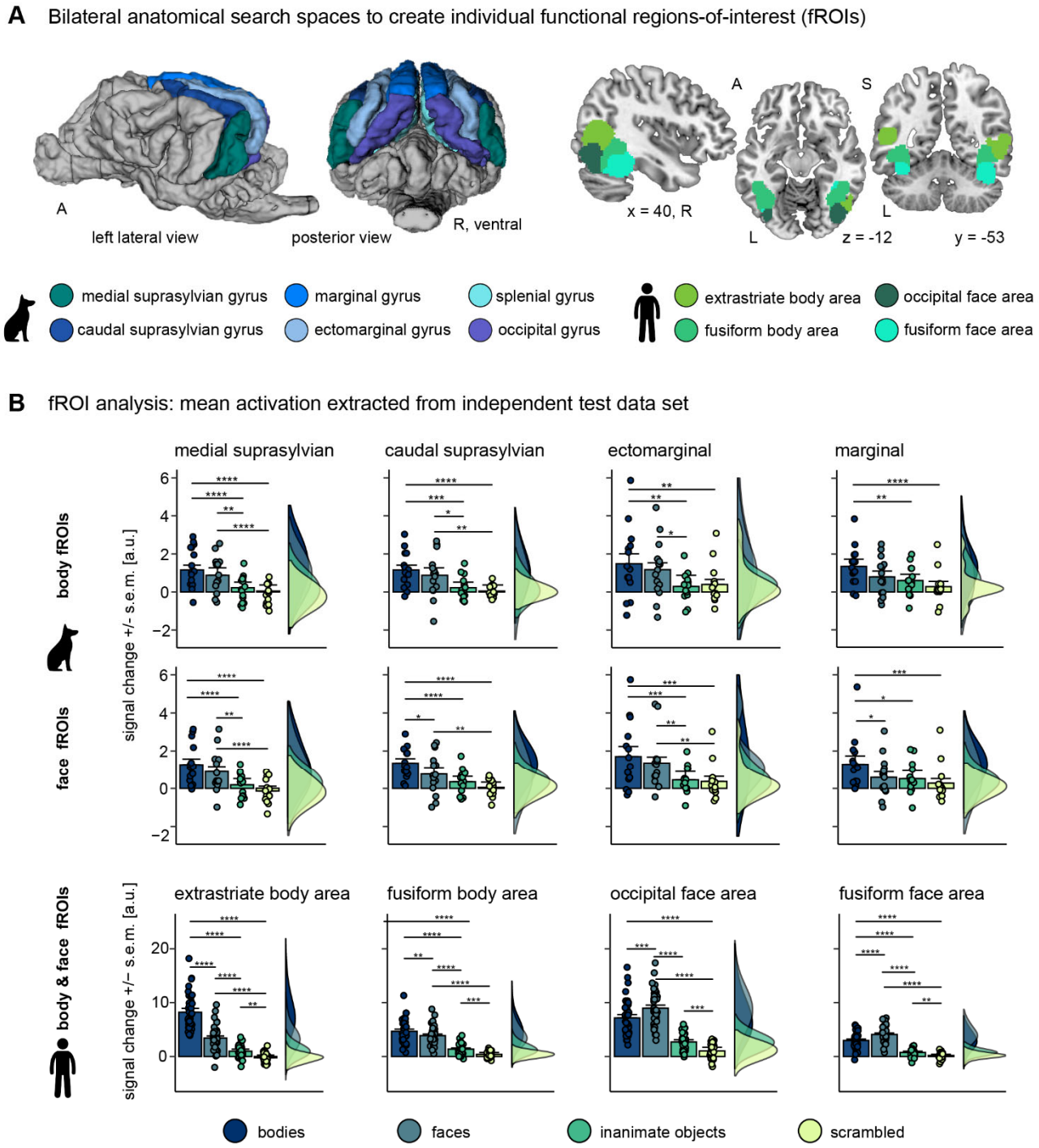

Fig 2. *Strongest activation levels for animate stimuli in both species, but differences between faces and bodies exclusive in humans.* (**A**) Based on the localizer data set, we defined individual category-specific regions-of-interest (functional region-of-interest approach, fROI) within multiple anatomically constrained search spaces using the contrasts bodies > inanimate objects (body fROIs) and faces > inanimate objects (face fROIs). (**B**) From these individual fROIs, we then extracted activation estimates during the viewing of faces, bodies, inanimate objects and scrambled images (all compared to the implicit baseline) using the data from the independent test data set to test potential face- or body-sensitivity. (**B**) In dogs, we observed increased activation levels for faces and bodies compared to inanimate objects or scrambled images in three occipito-temporal regions (medial and caudal suprasylvian, ectomarginal gyrus) in face and body fROIs. However, no difference between faces and bodies except in the caudal suprasylvian face fROI. The face and body fROIs located in the occipito-parietal marginal gyri resulted in increased activation levels primarily for bodies. In humans, similar to dogs, we observed the strongest activation levels for faces and bodies in all fROIs. In contrast to the dog data, the human data analysis consistently resulted in a significant activation change for bodies compared to faces in body fROIs and vice versa (**Table S2**). Planned comparisons were corrected for multiple comparisons using Tukey method. *$p < .05$, **$p < .01$, ***$p < .001$, ****$p < .0001$, s.e.m., standard error of the mean; a.u., arbitrary units. Atlas maps and search spaces refer to the dog brain atlas from Czeibert and colleagues [51] and human parcels were retrieved from previous work [56]. A, anterior; P, posterior; S, superior; L, left; R, right

2.2 Multivariate pattern analysis of animacy perception

Despite the overall activation (measured using mass-univariate analyses) to stimulus categories may not differ, we reasoned that more fine-grained analyses of multivariate activation patterns could reveal distinctions [59]. Therefore, we investigated the neural representations of faces and bodies in dogs and humans and their potential correspondence using whole-brain representational similarity analyses (RSA). We moved a 4 and 8 mm searchlight across the whole dog and human brain, respectively, in order to determine individual pattern similarity maps between all trials of each stimulus category [60–62] (**Fig 3A**). On the group-level, we then conducted paired *t*-tests to compare the pattern similarities maps of (1) animate vs. inanimate stimuli, (2) bodies vs. inanimate objects, (3) faces vs. inanimate objects, (4) faces vs. bodies, and (5,6) within the face and body categories: images of conspecifics vs. heterospecifics (i.e., dog faces vs. human faces; dog bodies vs. human bodies).

Results revealed increased (within-category) pattern similarity for animate compared to inanimate stimuli in the occipito-temporal cortex of dogs (i.e., caudal suprasylvian and splenial gyrus) and humans (i.e., middle occipital gyrus) overlapping with the identified fROIs. In human participants, we additionally observed increased similarity in the cerebellum and fronto-parietal regions (**Tables S4-S5**). In brief, this indicates distinct neural representations of animate compared to inanimate stimuli in higher-order visual regions of both species.

2.2.1 Similar and divergent neural representations for bodies and faces

Moving on to neural representations for bodies and faces, for bodies we observed increased pattern similarity compared to inanimate objects in higher-order visual areas in the occipito-temporal cortex, partially overlapping with the identified fROIs, and the cerebellum in both species (**Fig 3B**). Within the same regions (and again, in both

species), we also observed distinct activation patterns for conspecific compared to heterospecific bodies. Furthermore, when the dogs viewed dog bodies, results revealed increased similarity in limbic structures and regions associated with olfaction (**Fig 3C**). In humans, we observed increased similarity for human compared to dog bodies in fronto-parietal regions associated with action perception [63–65] (**Fig 3C**).

Observing faces compared to inanimate objects resulted in significantly increased pattern similarity in occipito-temporal cortices of both species and again in dog olfactory structures (**Fig 3D**). Comparing similarity patterns for faces vs. bodies, we only found significant differences for the human participants (see **Tables S4-5** for detailed results and **Fig S1** for a schematic summary of the main results).

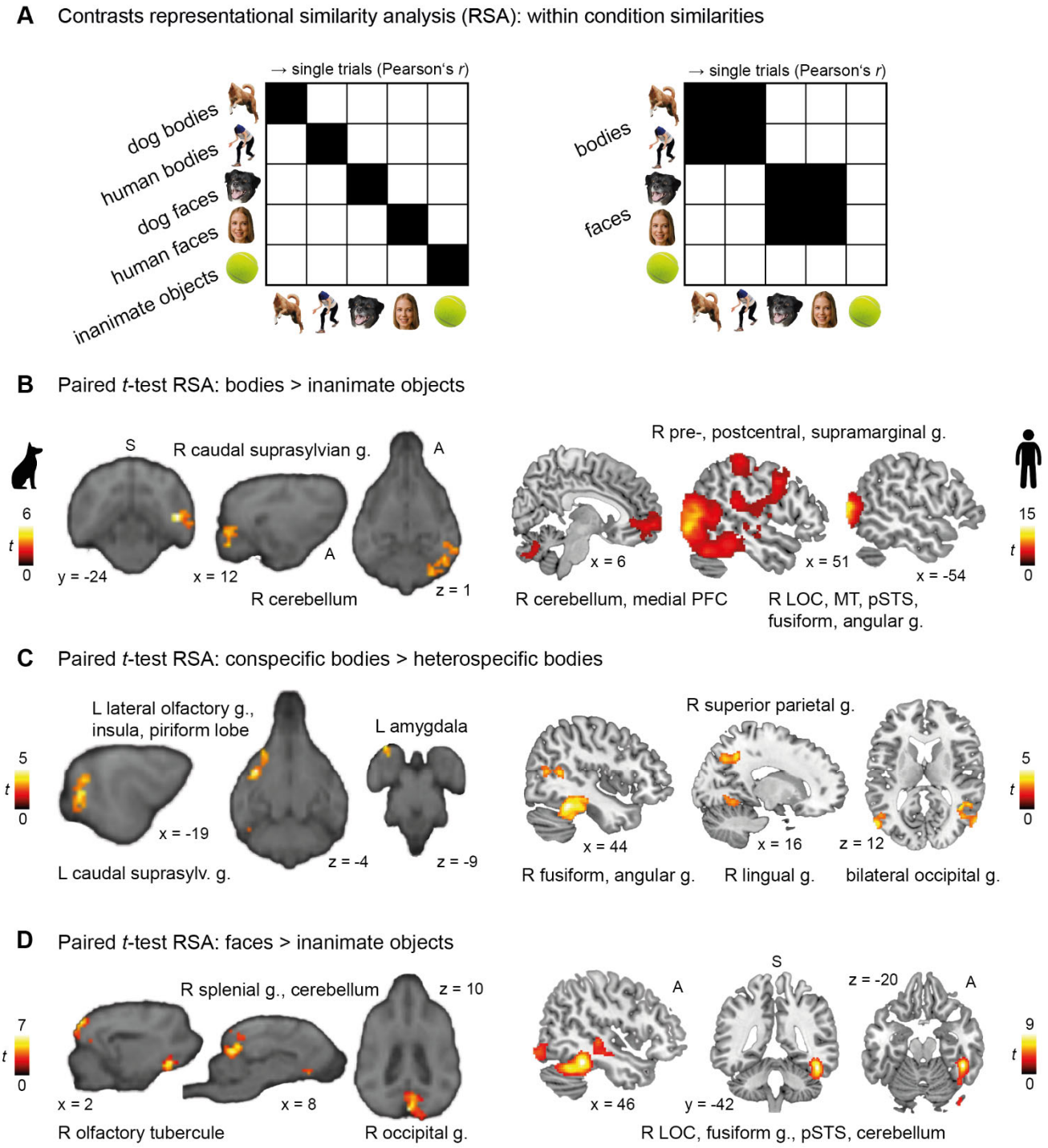

Fig 3. *Whole-brain representational similarity analysis (RSA) revealed similar and divergent neural patterns of activation for animate vs. inanimate stimuli but differences between faces and bodies again exclusive in human.* (**A**) We moved a 4/8 mm (dog/human) spherical searchlight across the whole brain to quantify the neural patterns underlying stimuli categories. Pattern similarity matrices were computed across the respective quadrants marked in black. (**B,D**) In both species, we observed increased pattern similarity for bodies or faces compared to inanimate stimuli in higher-order visual areas in the occipito-temporal cortex and the cerebellum. (**C,D**) In dogs we additionally detected distinct neural patterns of activation for faces and conspecific (= dog) bodies in olfactory and limbic regions. In humans, we observed an increased pattern similarity for (conspecific) bodies in fronto-parietal regions associated with action perception [63–65]. All results are displayed at $p < 0.05$ *FWE*-corrected at cluster-level, and using a cluster-defining threshold of $p < .005$ for the dog and $p < .001$ for the human data (**Tables S4-5**). Anatomical locations are shown in panel B for the dog and in D for the human data: superior (S), anterior (A); all sagittal, coronal and axial planes displayed have the same orientation. Coordinates refer to a canine-breed averaged template [50] or to MNI space for the human data. Person's *r*, correlation coefficient; t, *t*-value; g., gyrus; PFC, prefrontal cortex LOC, lateral occipital cortex; MT, middle temporal visual area (V5); pSTS, posterior superior temporal sulcus; R, right; L, left.

3 Discussion

Our findings revealed that the occipito-temporal cortex has a prominent role in the perception of animate entities in both dogs and humans. This suggests that the neural processing of animate vs. inanimate stimuli across mammalian brains may either have an old evolutionary origin in the common ancestors of canines and primates or is the result of convergent evolution [47]. However, within these regions, only humans displayed an additional sub-division into distinct face- and body-sensitive brain regions. Moreover, only dogs showed distinct responses to human and dog faces as well as dog bodies in olfactory areas (see **Fig S1** for summary of the results). These findings suggest a divergent evolution of the neural bases of face and body perception (or processing) in dogs and humans. The differential engagement of visual and olfactory brain functions would fit particularly well with the differential sensitivity and preferential use of these perceptual systems to infer social and contextual information.

Detecting biological agents is crucial for survival and social relationships. Hence, the visual differentiation between animate vs. inanimate entities is an evolutionary important category representation. Studies show that dogs target animate agents when, for example, presented with images of wild animals, humans or dogs embedded in natural landscapes [66] or of social interactions between humans and dogs [67]. Further, dividing stimuli into an animate vs. inanimate dimension is one of the first visually salient categorizations formed by human infants [68]. In this way, animacy representation provides the first building block for more complex visual categorizations such as faces vs. bodies. Thus, considering its biological significance and the observed cross-species similarities in our study, animacy might constitute a general organizing principle across mammalian brains.

Behavioural [7,33,34,43,69–72] and imaging studies [57,58] have also demonstrated that dogs are able to perceive facial and bodily cues of dogs and humans

and display high responsiveness to ostensive-referential bodily cues [44,45,73,74], already as puppies [75]. Our results do not contradict these findings, but suggest that visual regions involved in the perception of faces are also involved in the perception of other body parts, and may thus encode animate stimuli. A recent dog neuroimaging study [76] also showed that the visual regions observed in our study play a crucial part in the perception of complex social interactions, which would confirm their important role for social perception.

While previous investigations of how dogs perceive bodies have mainly focused on the decoding of human referential cues, we hope that our work will inspire more research on how dogs perceive bodily social as well as emotional cues of con- as well as heterospecifics. The absence of a further sub-specialization for face vs. body perception in the occipito-temporal cortex of dogs might indeed indicate that dogs in comparison to humans focus more on whole body social cues rather than on specific sub-parts. This interpretation is notably well in line with a recent comparative eye-tracking study [77].

Regarding species perception, our results indicate an increased salience for human compared to dog stimuli in humans, but no evidence for a conspecific-preference in the occipito-temporal cortex of dogs. Thus, human and dog stimuli appear to be equally salient for dogs. This is in line with previous behavioural studies suggesting, for example, no significant difference in the perception of human or dog emotional facial [34], whole-body cues [77], or images of social interactions [67]. Further, two recent studies demonstrated that dogs, already as puppies, follow human gestural-communication and show an interest in human faces [75], which has not been observed in wolf puppies [78]. Additionally, half of the variation in these socio-cognitive skills could be accounted for by genetic factors, suggesting that dogs' attention to humans might have been enhanced during domestication [75 for review of both

studies]. Future studies investigating species-preferences in dogs might thus consider adding further heterospecific stimuli of other familiar species, such as cats.

In accordance with a potential divergent evolution of face and body representations in dogs and humans, we also observed distinct neural representations for faces (regardless of species) and conspecific (dog) bodies in dog olfactory regions. Although unexpected, these results might reflect dogs' significantly higher olfactory sensitivity and its use to infer social and contextual information [54 for review]. However, the link between cognition and olfaction remains speculative since behavioural studies using olfactory cues so far mainly explored dogs' odour and disease detection abilities (e.g., [81–85]), while dog imaging studies on olfaction focused on reward-processing [86,87] or general sensory abilities [88–90]. However, a recent behavioural study investigating dog cognition using olfactory cues showed first evidence that dogs form representations of their owners when smelling their tracks [91].

In humans, results revealed distinct activation patterns for bodies in fronto-parietal regions that have been consistently associated with the perception of actions [63–65]. In dogs, we did not find activation in (pre-)motor cortices, but the increased neural sensitivity for bodies in the occipito-parietal marginal gyrus might be initial evidence for an analogous visual pathway to encode actions. However, this is beyond our study's scope, and the precise neural underpinnings of action observation in dogs have not yet been investigated.

We have taken several steps to maximize neural signal sensitivity already when designing our study (e.g., by using a block design) and at the analysis stage (e.g., by using dog-tailored hemodynamic models increasing response detection power [48]). Nevertheless, the extensive training required for dogs [49] resulted in different sample sizes for the two species, and the more extensive prior work in humans [56] resulted

in more constrained search spaces, and likely higher spatial sensitivity for the human data. Further, the majority (80%) of our pet dogs were pure-bred herding dogs, which prevented us from testing potential breed-specific differences and may limit generalizability.

In conclusion, our study reveals novel evidence for similarities and differences of animacy perception between two phylogenetically distant mammal species, advancing our understanding of the foundations of social cognition and behaviour. Finally, we provide insights into the differentially evolved sensory systems of dogs and humans for the perception of faces and bodies.

4 Materials and Methods

4.1 Participants

Fifteen pet dogs (*Canis familiaris*; 11 females, age range: 4-11 years, mean age: 7.8 years) consisting of 10 Border collies, 2 Australian shepherds, 1 Labrador retriever and 2 mixed-breed dogs and forty human participants (22 females, age range: 19-28 years, mean age: 23 years) participated in the present study.

Prior to MRI scanning, all dogs underwent initial medical examination concerning their eyesight and general health and received extensive training to habituate to the MRI environment [49]. They were fully awake, able to exit the MRI scanner at any time and equipped with noise protection (**Fig 1A**). All caregivers gave informed written consent to their dogs' participation. Human participants were right handed, had normal or corrected-to-normal vision, they reported no history of neurological or psychiatric disease, nor phobia of dogs, fulfilled the standard inclusion criteria for functional MRI, and gave informed written consent to participate. Dog data collection was approved by the institutional ethics and animal welfare commission in accordance with Good Scientific Practice (GSP) guidelines and national legislation at the University of Veterinary Medicine Vienna (ETK-06/06/2017), based on a pilot study conducted at

the University of Vienna. Human data collection was approved by the ethics committee of the University of Vienna (reference number: 00565) and performed in line with the latest revision of the Declaration of Helsinki (2013).

4.2 Task and procedure

We employed a block design (duration: 12 s) split in two 5 min runs where participants saw images of faces and bodies of dogs or humans, objects and scrambled versions of these images (5 images per block; **Fig 1B**, see below) on an MR-compatible screen (32 inch) positioned at the end of the scanner bore. Crucially, we used the same task for dogs and humans. Human participants were instructed to watch the images presented on the MR screen and dogs were trained to attend to the MR screen (passive viewing paradigm). Each run contained three blocks per condition, block order was randomized but the same condition was never presented twice in a row. Between blocks, participants saw a visual baseline jittered between 3-7 s with a white cross presented on a grey background. Image composition for each block and order within each block was randomized across participants to ensure effects are not driven by specific blocks; each image was presented once. The task was implemented using PsychoPy [92]. Overall motion and wakefulness were live monitored via the camera of an eye-tracker (Eyelink 1000 Plus, SR Research, Ontario, Canada) positioned below the MR-compatible screen. For the dogs, the trainer stayed within the scanner room but out-of-sight throughout the scan session to monitor and handle the dogs. Human participants saw both runs within a single scanner session with a short break in-between. For the dogs, the number of attempted sessions varied depending on how many repetitions they needed to complete one run without substantive motion and with sufficient attentiveness (i.e., eyes open and gazing towards the centre of the screen); in-between task runs the dogs always were given a short break outside the MR scanner. Realignment parameters were evaluated after each scan session. If

overall motion exceeded 4 mm in any of the three translation directions, the dog was re-invited to repeat the run in a subsequent session and sessions were scheduled at least one week apart. On average, dogs needed three sessions to complete both runs. No data of the non-successful sessions were used for analysis.

4.2.1 Stimulus material

The stimulus set comprised 180 coloured images of faces and bodies of dogs and humans, everyday inanimate objects (e.g., a toy, a chair), and phase-grid scrambled versions of each category (30 images per condition) derived from Wagner and colleagues [93], the Hemera Photo-Object data base (Hemera Technologies) and the internet (see **Fig 1B** for examples). The images were resized to 600 × 600 pixels and presented in the centre of the MR screen on grey background. We cut out the heads off from the body images, as well as objects from body images (e.g., a coffee cup, a soccer ball). The images showed a variety of postures (e.g., jumping, looking up), neutral and positive emotional displays (e.g., sleeping, smiling) and viewing perspectives (e.g., from above, from a side angle). Luminance was set homogeneously across stimuli and we controlled for spatial extent (see supporting information for details).

4.3 MRI data acquisition

We acquired all MRI data with a 3T Siemens Skyra MR-system (Siemens Medical, Erlangen, Germany) and a 15-channel coil (initially designed for measurements of the human knee) for data acquisition in dogs and a 32-channel human head coil for data acquisition in humans. Functional scans of dogs used a 2-fold multiband (MB) accelerated echo planar imaging (EPI) sequence including the following parameters: voxel size = 1.5 x 1.5 x 2 mm^3, repetition time (TR) / echo time (TE) = 1000/38 ms, field of view (FoV) = 144 × 144 × 58 mm^3, flip angle = 61°, 20%

gap and 24 axial slices covering the whole brain (interleaved acquisition, descending order). Structural scans had a voxel size of 0.7 mm isotropic (TR/TE = 2100/3.13 ms, FoV = 230 × 230 × 165 mm^3) and were acquired in a separate scan session prior to functional data collection. Human functional scans were acquired using a 4-fold MB accelerated EPI sequence including the following parameters: voxel size = 2 mm isotropic, TR/TE = 1200/34 ms, FoV = 192 × 192 × 124.8 mm^3, flip angle = 66°, 20% gap and 52 axial slices coplanar to the connecting line between anterior and posterior commissure (interleaved acquisition, ascending order). Additionally, we obtained field map scans to correct functional scans for magnetic field inhomogeneities using a double echo gradient echo sequence with the following parameters: voxel size = 1.72 x 1.72 x 3.85 mm^3, TR/TE1/TE2 = 400/4.92/7.38 ms, FoV = 220 × 220 × 138 mm^3, flip angle = 60° and 36 axial slices (same orientation as functional scans). Structural scans had a voxel size of 0.8 mm isotropic (TR/TE = 2300/2.43 ms, FoV = 256 × 256 × 166 mm^3) and were acquired after functional data acquisition.

4.4 Data processing and statistical analysis

Imaging data was preprocessed and analyzed using SPM12 (https://www.fil.ion.ucl.ac.uk/spm/software/spm12/), Matlab 2018b (MathWorks) and R 3.6.3 [94].

4.4.1 MRI data preprocessing

In both samples, we slice-time corrected (reference: middle slice) and realigned functional images to the mean image. Human imaging data was also unwarped using the acquired field map. Dog imaging data was manually reoriented with the rostral commissure set as a visual reference (SPM module: "*Reorient images / Set origin*") to match the template orientation [50] and structural images were skull-stripped using individual binary brain masks created using itk-SNAP [95]. Next, we co-registered the

structural and functional images to the mean functional image, segmented the structural images in both samples and normalized the human data to the Montreal Neurological Institute (MNI) template space and the dog data to a breed-averaged stereotaxic template space [50]. Normalized images were resliced to 1.5 mm isotropic and smoothed with a 3-dimensional Gaussian kernel (full-width-at-half-maximum, FWHM; with twice the raw voxel resolution: dogs/humans = 3/4 mm; see [48] for an in-depth description of our dog data preprocessing pipeline). We then calculated individual scan-to-scan motion (frame wise displacement, FD) and added motion regressors to first-level GLMs for each scan exceeding the a priori set FD threshold of 0.5 mm (motion scrubbing [96,97]) to account for both translational and rotational displacements. For the dog participants, we removed on average 8% of the scans from each run (run 1: mean FD = 0.23 mm, 90th percentile = 0.36 mm; run 2: mean FD = 0.24 mm, 90th percentile = 0.38 mm) and 1% of the scans from each run of the human participants (run 1: mean FD = 0.17 mm, 90th percentile = 0.22 mm; run 2: mean FD = 0.18 mm, 90th percentile = 0.21 mm).

4.4.2 fMRI data analysis

Mass-univariate activation analysis. We analysed the functional data using a general linear model (GLM) approach implemented in SPM12. Individual GLM matrices included six regressors of interest for task (dog faces, dog bodies, human faces, human bodies, inanimate objects, scrambled) and the six regressors from the realignment procedure (see above) were added as nuisance regressors. All blocks were estimated using a boxcar function time-locked to the onset of each block with a duration of 12 s. For the dog data, the signal was convolved with a tailored dog haemodynamic response function [48] (HRF), while the standard human canonical HRF (i.e., the default HRF parameters provided by SPM12) was used for the human data. The dog HRF reflects a previously observed 2-3 s earlier peak of the BOLD signal

than expected by the human HRF model [48]. Normalized, individual binary masks served as explicit masks and we applied a high-pass filter with a cut-off at 128 s. We then split the data in two sets (task run 1, task run 2). Based on the data from the first task run, we estimated three subject-level contrast maps for the difference between our conditions of interest (i.e., faces, bodies with equal weights for human and dog images) and objects, and a visual stimulation contrast (all conditions > implicit visual baseline). For the second task run, we computed eight subject-level contrasts, one for each task regressor (i.e., dog bodies, human bodies, dog faces, human faces, everyday inanimate objects, scrambled), averaged for faces (i.e., dog and human faces) and averaged for bodies (i.e., dog and human bodies) compared to implicit visual baseline.

Functional region of interest (fROI) approach. We implemented a standard functional region-of-interest (fROI, [53–55]) approach to investigate potential category-specificity of cortical regions. This approach allows us to directly test the potential category-sensitivity quantified by increased activation level while accounting for slight differences in the location of activation peaks between individuals as which have been reported in previous dog imaging studies [40,42].

The participant-level contrast images from the first run served as localizer data to define individual category-sensitive regions. Within anatomically constrained search spaces (**Fig 2A**) we selected the top-10% voxel from each hemisphere with the strongest signal for the condition-of-interest (i.e., face areas: faces > objects, body areas: bodies > objects) to form bilateral individual fROIs. Selecting the top-10% voxel was an *a priori* decision we made because the resulting fROI sizes (on average: 30 voxels) were similar to the average cluster size observed in a previous dog imaging study that used two visual paradigms and the same smoothing kernel [48]. Further, percentages instead of absolute numbers took also the varying search space sizes

into account (see **supporting material** and **Fig S2-3** for more information). The data from the left out second task run allowed then to directly test potential category specificity in an independent data set. Thus, we extracted the activation levels from the conditions-of-interest contrasted against implicit visual baseline from both body and faces areas (= individual fROIs).

Group functional ROI analyses were performed running repeated measures analyses of variance (ANOVAs). First, we tested our main research question, whether the body areas resulted in increased sensitivity for bodies regardless of species and vice versa for faces, and added everyday objects and scrambled images as further conditions. Thus, we ran a one-way ANOVA with *stimuli category* (faces, bodies, everyday objects, scrambled*)* as dependent variable. Next, to investigate if there is a difference in activation between conspecific and heterospecific stimuli, we used 2 x 2 within-subjects ANOVAs (*species*: conspecific, heterospecific; *image category*: face, body). *P*-values for group comparisons investigating the same research questions were Bonferroni-adjusted, e.g., if the 6 potential body fROIs result in increased sensitivity for bodies compared to all other categories results in an adjusted *p*-value of 0.008 (= 0.05/6). Adjusted *p*-values are reported along with the results (**Tables S2-3**). For whole-brain group analyses, we tested significance applying a whole-brain familywise error (*FWE*) correction for the human data and a cluster-level inference with a cluster defining threshold of $p < 0.001$ and a cluster probability of $p < 0.05$ *FWE* corrected for multiple comparisons for the dog data. Cluster extent (i.e., minimum spatial extend to be labelled significant) was calculated using the SPM extension "CorrClusTh.m" (by Thomas Nichols, University of Warwick, United Kingdom, and Marko Wilke, University of Tübingen, Germany; https://warwick.ac.uk/fac/sci/statistics/staff/academic-research/nichols/scripts/spm/).

Representational similarity analysis. Next, we investigated the neural representations for faces, bodies and objects and their potential convergence in dogs and humans. To this end, we performed a whole-brain representational similarity analysis (RSA; [60–62]) to determine neural pattern similarities within image categories. GLMs were modelled identical to univariate GLMs (see above) but for each block, we ran a separate GLM with the block as task regressor and remaining blocks were combined in one regressor of no interest [98]; runs were modelled independently. Thus, the analysis resulted in 36 beta images for each participant (6 conditions × 6 trials). RSA was performed using the smoothed functional data. For all RSA analyses, we moved a spherical searchlight [99] (dogs: r = 4 mm, 81 voxel; humans: r = 8 mm, 251 voxel) throughout individual whole-brain grey matter masks computed based on the normalised segmentation output considering only searchlights with a minimum of 15 grey matter voxel for the dog and 30 for the human data.

Within a given searchlight, we extracted single-trial beta estimates from all voxels and sorted them according to their stimuli category (**Fig 3A**; dog / human bodies, dog / human faces, inanimate objects) and reshaped the data to a trial × voxel matrix. Next, we z-scored the data across trials and runs and computed a trial × trial similarity matrix by correlating each beta estimate of each trial to all other trial estimates. Finally, in order to retrieve overall similarity scores, we then Fisher's z-transformed the data and calculated overall similarity matrices by averaging scores across the respective quadrants. We were specifically interested in pattern similarities across animate vs. inanimate (faces × bodies vs. inanimate objects), faces or bodies vs. inanimate objects, faces vs. bodies and conspecific vs. heterospecific species dimensions within face and body categories. We then assigned the overall similarity values to the centre voxel of each searchlight resulting in individual whole-brain pattern similarity maps.

On the group-level, we then used paired *t*-tests to compare the pattern similarities between trials of (1) faces vs. inanimate objects (i.e., [dog faces × human faces] vs. inanimate objects), (2) bodies vs. inanimate objects (i.e., [dog bodies × human bodies] vs. inanimate objects), (3) animate vs. inanimate images (i.e., [dog faces × human faces x dog bodies × human bodies] vs. inanimate objects), (4) faces vs. bodies (i.e., [dog faces × human faces] vs. [dog bodies × human bodies]), and (5,6) within the face and body categories: images of conspecifics vs. heterospecifics (i.e., dog faces vs. human faces; dog bodies vs. human bodies). We computed permutation tests [100] to determine group-level significance using the Statistical nonParametric Mapping (SnPm13) toolbox running 5000 permutations for each paired *t*-test and applied cluster-level inference with a cluster defining threshold of $p < .005/.001$ (dogs/humans) and a cluster probability of $p < 0.05$ familywise error corrected (*FWE*) for multiple comparisons.

Data visualization. Data was visualized using SPM12 (https://www.fil.ion.ucl.ac.uk/spm/software/spm12/), Matlab 2018b (MathWorks), itk-SNAP [95], R 3.6.3 [94] with mainly the packages ggplot2 [101] and RainCloudPlots [102] and the python project nilearn (http://nilearn.github.io).

5 Acknowledgments

We thank Prof. Nancy Kanwisher for her helpful comments on the preliminary results and analysis plan. We also want to thank Morris Krainz, Anna Thallinger, Olaf Borghi and Helena Manzenreiter for their help collecting the data, Boryana Todorova for her support in preparing the stimuli set and all the dogs and their caregivers and all human participants for taking part in this project. This project was supported by the Austrian Science Fund (FWF): W1262-B29 and by the Vienna Science and Technology Fund (WWTF), the City of Vienna and ithuba Capital AG through project CS18-012 , and the Messerli Foundation (Sörenberg, Switzerland). The funders had

no role in study design, data collection and analysis, decision to publish, or preparation of the manuscript.

6 CRediT authorship statement

Magdalena Boch: Conceptualization, Methodology, Software, Validation, Formal analysis, Investigation, Data curation, Writing - original draft, Writing - review & editing, Visualization, Project administration. **Isabella C. Wagner**: Conceptualization, Methodology, Resources, Writing - original draft, Writing - review & editing, Supervision. **Sabrina Karl**: Investigation, Writing - review & editing. **Ludwig Huber**: Conceptualization, Resources, Writing - review & editing, Supervision, Funding acquisition. **Claus Lamm**: Conceptualization, Methodology, Resources, Writing - original draft, Writing - review & editing, Supervision, Funding acquisition.

7 Declaration of Competing Interests

The authors declare no competing financial interests.

8 References

1. Rajhans P, Jessen S, Missana M, Grossmann T. Putting the face in context: Body expressions impact facial emotion processing in human infants. Dev Cogn Neurosci. 2016;19: 115–121. doi:10.1016/J.DCN.2016.01.004
2. Aviezer H, Trope Y, Todorov A. Body cues, not facial expressions, discriminate between intense positive and negative emotions. Science. 2012;338: 1225–1229. doi:10.1126/science.1224313
3. Barrett LF, Mesquita B, Gendron M. Context in emotion perception. Curr Dir Psychol Sci. 2011;20: 286–290. doi:10.1177/0963721411422522
4. Lecker M, Dotsch R, Bijlstra G, Aviezer H. Bidirectional contextual influence between faces and bodies in emotion perception. Emotion. 2020;20: 1154–1164. doi:10.1037/EMO0000619
5. Poyo Solanas M, Zhan M, Vaessen M, Hortensius R, Engelen T, de Gelder B. Looking at the face and seeing the whole body. Neural basis of combined face and body expressions. Soc Cogn Affect Neurosci. 2018;13: 135–144. doi:10.1093/scan/nsx130
6. de Gelder B, de Borst AW, Watson R. The perception of emotion in body expressions. Wiley Interdiscip Rev Cogn Sci. 2015;6: 149–158. doi:10.1002/wcs.1335
7. Müller CA, Schmitt K, Barber ALA, Huber L. Dogs can discriminate emotional expressions of human faces. Curr Biol. 2015;25: 601–605. doi:10.1016/j.cub.2014.12.055
8. Kravitz DJ, Saleem KS, Baker CI, Ungerleider LG, Mishkin M. The ventral visual pathway: An expanded neural framework for the processing of object quality. Trends Cogn Sci. 2013;17: 26–49. doi:10.1016/j.tics.2012.10.011
9. Ungerleider LG, Haxby J V. “What” and “where” in the human brain. Curr Opin Neurobiol. 1994;4: 157–165. doi:10.1016/0959-4388(94)90066-3
10. Schwarzlose RF, Baker CI, Kanwisher N. Separate face and body selectivity on the fusiform gyrus. J Neurosci. 2005;25: 11055–11059. doi:10.1523/JNEUROSCI.2621-05.2005
11. Peelen M V., Downing PE. Selectivity for the human body in the fusiform gyrus. J Neurophysiol. 2005;93: 603–608. doi:10.1152/jn.00513.2004
12. Peelen M V., Downing PE. The neural basis of visual body perception. Nat Rev Neurosci. 2007;8: 636–648. doi:10.1038/nrn2195
13. Downing PE, Jiang Y, Shuman M, Kanwisher N. A cortical area selective for visual processing of the human body. Science. 2001;293: 2470–2473. doi:10.1126/science.1063414
14. Spiridon M, Fischl B, Kanwisher N. Location and spatial profile of category-specific regions in human extrastriate cortex. Hum Brain Mapp. 2006;27: 77–89. doi:10.1002/hbm.20169
15. Kanwisher N. Domain specificity in face perception. Nat Neurosci. 2000;3: 759–763. doi:10.1038/77664
16. Yovel G, Kanwisher N. Face perception: domain specific, not process specific. Neuron. 2004;44: 889–898. doi:10.1016/j.neuron.2004.11.018
17. Wegrzyn M, Riehle M, Labudda K, Woermann F, Baumgartner F, Pollmann S, et al. Investigating the brain basis of facial expression perception using multi-voxel pattern analysis. Cortex. 2015;69: 131–140. doi:10.1016/J.CORTEX.2015.05.003

18. Wiggett AJ, Pritchard IC, Downing PE. Animate and inanimate objects in human visual cortex: Evidence for task-independent category effects. Neuropsychologia. 2009;47: 3111–3117. doi:10.1016/J.NEUROPSYCHOLOGIA.2009.07.008
19. Chao LL, Haxby J V., Martin A. Attribute-based neural substrates in temporal cortex for perceiving and knowing about objects. Nat Neurosci. 1999;2: 913–919. doi:10.1038/13217
20. Downing PE, Chan AW-Y, Peelen M V., Dodds CM, Kanwisher N. Domain specificity in visual cortex. Cereb Cortex. 2006;16: 1453–1461. doi:10.1093/CERCOR/BHJ086
21. Kanwisher N, Yovel G. The fusiform face area: a cortical region specialized for the perception of faces. Philos Trans R Soc B Biol Sci. 2006;361: 2109–2128. doi:10.1098/rstb.2006.1934
22. Tsao DY, Freiwald WA, Tootell RBH, Livingstone MS. A cortical region consisting entirely of face-selective cells. Science. 2006;311: 670–674. doi:10.1126/science.1119983
23. Tsao DY, Moeller S, Freiwald WA. Comparing face patch systems in macaques and humans. Proc Natl Acad Sci U S A. 2008;105: 19514–19519. doi:10.1073/pnas.0809662105
24. Tsao DY, Freiwald WA, Knutsen TA, Mandeville JB, Tootell RBH. Faces and objects in macaque cerebral cortex. Nat Neurosci. 2003;6: 989–995. doi:10.1038/nn1111
25. Desimone R, Albright TD, Gross CG, Bruce C. Stimulus-selective properties of inferior temporal neurons in the macaque. J Neurosci. 1984;4: 2051–2062. doi:10.1523/jneurosci.04-08-02051.1984
26. Wachsmuth E, Oram MW, Perrett DI. Recognition of objects and their component parts: Responses of single units in the temporal cortex of the macaque. Cereb Cortex. 1994;4: 509–522. doi:10.1093/cercor/4.5.509
27. Gross CG, Bender DB, Rocha-Miranda CE. Visual receptive fields of neurons in inferotemporal cortex of the monkey. Science. 1969;166: 1303–1306. doi:10.1126/science.166.3910.1303
28. Haxby J V., Horwitz B, Ungerleider LG, Maisog JM, Pietrini P, Grady CL. The functional organization of human extrastriate cortex: a PET-rCBF study of selective attention to faces and locations. J Neurosci. 1994;14: 6336–6353. doi:10.1523/JNEUROSCI.14-11-06336.1994
29. Bunford N, Hernández-Pérez R, Farkas EB, Cuaya L V., Szabó D, Szabó ÁG, et al. Comparative Brain Imaging Reveals Analogous and Divergent Patterns of Species and Face Sensitivity in Humans and Dogs. J Neurosci. 2020;40: 8396–8408. doi:10.1523/JNEUROSCI.2800-19.2020
30. Kanwisher N, Stanley D, Harris A. The fusiform face area is selective for faces not animals. Neuroreport. 1999;10: 183–187. doi:10.1097/00001756-199901180-00035
31. Pinsk MA, Arcaro M, Weiner KS, Kalkus JF, Inati SJ, Gross CG, et al. Neural representations of faces and body parts in macaque and human cortex: a comparative fMRI study. J Neurophysiol. 2009;101: 2581–2600. doi:10.1152/jn.91198.2008
32. Racca A, Amadei E, Ligout S, Guo K, Meints K, Mills D. Discrimination of human and dog faces and inversion responses in domestic dogs (Canis familiaris). Anim Cogn. 2010;13: 525–533. doi:10.1007/s10071-009-0303-3
33. Huber L, Racca A, Scaf B, Virányi Z, Range F. Discrimination of familiar human faces in dogs (Canis familiaris). Learn Motiv. 2013;44: 258–269. doi:10.1016/J.LMOT.2013.04.005
34. Albuquerque N, Guo K, Wilkinson A, Savalli C, Otta E, Mills D. Dogs recognize dog and human emotions. Biol Lett. 2016;12: 20150883. doi:10.1098/rsbl.2015.0883

35. Huber L. How Dogs Perceive and Understand Us. Curr Dir Psychol Sci. 2016;25: 339–344. doi:10.1177/0963721416656329
36. Maginnity ME, Grace RC. Visual perspective taking by dogs (Canis familiaris) in a Guesser–Knower task: evidence for a canine theory of mind? Anim Cogn. 2014;17: 1375–1392. doi:10.1007/s10071-014-0773-9
37. Catala A, Mang B, Wallis L, Huber L. Dogs demonstrate perspective taking based on geometrical gaze following in a Guesser–Knower task. Anim Cogn. 2017;20: 581–589. doi:10.1007/s10071-017-1082-x
38. Bunford N, Andics A, Kis A, Miklósi Á, Gácsi M. Canis familiaris As a Model for Non-Invasive Comparative Neuroscience. Trends Neurosci. 2017;40: 438–452. doi:10.1016/J.TINS.2017.05.003
39. Szabó D, Gábor A, Gácsi M, Faragó T, Kubinyi E, Miklósi Á, et al. On the Face of It: No Differential Sensitivity to Internal Facial Features in the Dog Brain. Front Behav Neurosci. 2020;14. doi:10.3389/fnbeh.2020.00025
40. Dilks DD, Cook PF, Weiller SK, Berns HP, Spivak M, Berns GS. Awake fMRI reveals a specialized region in dog temporal cortex for face processing. PeerJ. 2015; 3:e1115. doi:10.7717/peerj.1115
41. Thompkins AM, Ramaiahgari B, Zhao S, Gotoor SSR, Waggoner P, Denney TS, et al. Separate brain areas for processing human and dog faces as revealed by awake fMRI in dogs (Canis familiaris). Learn Behav. 2018;46: 561–573. doi:10.3758/s13420-018-0352-z
42. Cuaya L V., Hernández-Pérez R, Concha L. Our faces in the dog's brain: Functional imaging reveals temporal cortex activation during perception of human faces. PLoS One. 2016;11: e0149431. doi:10.1371/journal.pone.0149431
43. Siniscalchi M, Lusito R, Vallortigara G, Quaranta A. Seeing Left- or Right-Asymmetric Tail Wagging Produces Different Emotional Responses in Dogs. Curr Biol. 2013;23: 2279–2282. doi:10.1016/J.CUB.2013.09.027
44. Duranton C, Range F, Virányi Z. Do pet dogs (Canis familiaris) follow ostensive and non-ostensive human gaze to distant space and to objects? R Soc Open Sci. 2017;4: 170349. doi:10.1098/rsos.170349
45. Topál J, Kis A, Oláh K. Dogs' Sensitivity to Human Ostensive Cues: A Unique Adaptation? The Social Dog: Behavior and Cognition. Elsevier Inc.; 2014. pp. 319–346. doi:10.1016/B978-0-12-407818-5.00011-5
46. Bräuer J, Kaminski J, Riedel J, Call J, Tomasello M. Making inferences about the location of hidden food: Social dog, causal ape. J Comp Psychol. 2006;120: 38–47. doi:10.1037/0735-7036.120.1.38
47. Fitch WT, Huber L, Bugnyar T. Social Cognition and the Evolution of Language: Constructing Cognitive Phylogenies. Neuron. 2010;65: 795–814. doi:10.1016/J.NEURON.2010.03.011
48. Boch M, Karl S, Sladky R, Huber L, Lamm C, Wagner IC. Tailored haemodynamic response function increases detection power of fMRI in awake dogs (Canis familiaris). Neuroimage. 2021;224: 117414. doi:10.1016/j.neuroimage.2020.117414
49. Karl S, Boch M, Virányi Z, Lamm C, Huber L. Training pet dogs for eye-tracking and awake fMRI. Behav Res Methods. 2020;52. doi:10.3758/s13428-019-01281-7

50. Nitzsche B, Boltze J, Ludewig E, Flegel T, Schmidt MJ, Seeger J, et al. A stereotaxic breed-averaged, symmetric T2w canine brain atlas including detailed morphological and volumetrical data sets. Neuroimage. 2019;187: 93–103. doi:10.1016/j.neuroimage.2018.01.066
51. Czeibert K, Andics A, Petneházy Ö, Kubinyi E. A detailed canine brain label map for neuroimaging analysis. Biol Futur. 2019;70: 112–120. doi:10.1556/019.70.2019.14
52. Shattuck DW, Mirza M, Adisetiyo V, Hojatkashani C, Salamon G, Narr KL, et al. Construction of a 3D probabilistic atlas of human cortical structures. Neuroimage. 2008;39: 1064–1080. doi:10.1016/j.neuroimage.2007.09.031
53. Fedorenko E, Hsieh P-J, Nieto-Castañón A, Whitfield-Gabrieli S, Kanwisher N. New method for fMRI investigations of language: Defining ROIs functionally in individual subjects. J Neurophysiol. 2010;104: 1177–1194. doi:10.1152/jn.00032.2010
54. Poldrack RA. Region of interest analysis for fMRI. Soc Cogn Affect Neurosci. 2007;2: 67–70. doi:10.1093/scan/nsm006
55. Saxe R, Brett M, Kanwisher N. Divide and conquer: A defense of functional localizers. Neuroimage. 2006;30: 1088–1096. doi:10.1016/J.NEUROIMAGE.2005.12.062
56. Julian JB, Fedorenko E, Webster J, Kanwisher N. An algorithmic method for functionally defining regions of interest in the ventral visual pathway. Neuroimage. 2012;60: 2357–2364. doi:10.1016/j.neuroimage.2012.02.055
57. Karl S, Boch M, Zamansky A, van der Linden D, Wagner IC, Völter CJ, et al. Exploring the dog–human relationship by combining fMRI, eye-tracking and behavioural measures. Sci Rep. 2020;10: 22273. doi:10.1038/s41598-020-79247-5
58. Thompkins AM, Lazarowski L, Ramaiahgari B, Gotoor SSR, Waggoner P, Denney TS, et al. Dog–human social relationship: representation of human face familiarity and emotions in the dog brain. Anim Cogn. 2021;24: 251–266. doi:10.1007/s10071-021-01475-7
59. Cohen MA, Dilks DD, Koldewyn K, Weigelt S, Feather J, Kell AJE, et al. Representational similarity precedes category selectivity in the developing ventral visual pathway. Neuroimage. 2019;197: 565–574. doi:10.1016/j.neuroimage.2019.05.010
60. Kriegeskorte N, Kievit RA. Representational geometry: integrating cognition, computation, and the brain. Trends Cogn Sci. 2013;17: 401–412. doi:10.1016/J.TICS.2013.06.007
61. Kriegeskorte N, Mur M, Bandettini P. Representational similarity analysis - connecting the branches of systems neuroscience. Front Syst Neurosci. 2008;2. doi:10.3389/neuro.06.004.2008
62. Kriegeskorte N, Mur M, Ruff DA, Kiani R, Bodurka J, Esteky H, et al. Matching Categorical Object Representations in Inferior Temporal Cortex of Man and Monkey. Neuron. 2008;60: 1126–1141. doi:10.1016/J.NEURON.2008.10.043
63. Rizzolatti G, Fogassi L, Gallese V. Neurophysiological mechanisms underlying the understanding and imitation of action. Nat Rev Neurosci. 2001;2: 661–670. doi:10.1038/35090060
64. Hamilton AF de C, Grafton ST. Goal Representation in Human Anterior Intraparietal Sulcus. J Neurosci. 2006;26: 1133–1137. doi:10.1523/JNEUROSCI.4551-05.2006
65. Kilner JM, Neal A, Weiskopf N, Friston KJ, Frith CD. Evidence of Mirror Neurons in Human Inferior Frontal Gyrus. J Neurosci. 2009;29: 10153–10159. doi:10.1523/JNEUROSCI.2668-

09.2009

66. Törnqvist H, Somppi S, Kujala M V., Vainio O. Observing animals and humans: Dogs target their gaze to the biological information in natural scenes. PeerJ. 2020;8: e10341. doi:10.7717/peerj.10341
67. Törnqvist H, Somppi S, Koskela A, Krause CM, Vainio O, Kujala M V. Comparison of dogs and humans in visual scanning of social interaction. R Soc Open Sci. 2015;2: 150341. doi:10.1098/rsos.150341
68. Spriet C, Abassi E, Hochmann J-R, Papeo L. Visual object categorization in infancy. bioRxiv. 2021; 2021.02.25.432436. doi:10.1101/2021.02.25.432436
69. Buttelmann D, Tomasello M. Can domestic dogs (Canis familiaris) use referential emotional expressions to locate hidden food? Anim Cogn. 2013. doi:10.1007/s10071-012-0560-4
70. Nagasawa M, Murai K, Mogi K, Kikusui T. Dogs can discriminate human smiling faces from blank expressions. Anim Cogn. 2011;14: 525–533. doi:10.1007/s10071-011-0386-5
71. Barber ALA, Randi D, Müller CA, Huber L. The Processing of Human Emotional Faces by Pet and Lab Dogs: Evidence for Lateralization and Experience Effects. Guo K, editor. PLoS One. 2016;11: e0152393. doi:10.1371/journal.pone.0152393
72. Racca A, Guo K, Meints K, Mills DS. Reading Faces: Differential Lateral Gaze Bias in Processing Canine and Human Facial Expressions in Dogs and 4-Year-Old Children. PLoS One. 2012;7: e36076. doi:10.1371/journal.pone.0036076
73. Range F, Viranyi Z, Huber L. Selective Imitation in Domestic Dogs. Curr Biol. 2007;17: 868–872. doi:10.1016/J.CUB.2007.04.026
74. Soproni K, Miklósi Á, Topál J, Csányi V. Dogs' (Canis familiaris) Responsiveness to Human Pointing Gestures. J Comp Psychol. 2002;116: 27–34. doi:10.1037//0735-7036.116.1.27
75. Bray EE, Gnanadesikan GE, Horschler DJ, Levy KM, Kennedy BS, Famula TR, et al. Early-emerging and highly heritable sensitivity to human communication in dogs. Curr Biol. 2021;31: 1–5. doi:10.1016/j.cub.2021.04.055
76. Karl S, Sladky R, Lamm C, Huber L. Neural Responses of Pet Dogs Witnessing their caregiver's Positive Interactions with a Conspecific: An fMRI Study. Cereb Cortex Commun. 2021;tgab047. doi:10.1093/TEXCOM/TGAB047
77. Correia-Caeiro C, Guo K, Mills D. Bodily emotional expressions are a primary source of information for dogs, but not for humans. Anim Cogn. 2021;1: 3. doi:10.1007/s10071-021-01471-x
78. Salomons H, Smith KCM, Callahan-Beckel M, Callahan M, Levy K, Kennedy BS, et al. Cooperative Communication with Humans Evolved to Emerge Early in Domestic Dogs. Curr Biol. 2021;31: 3137-3144.e11. doi:10.1016/J.CUB.2021.06.051
79. Kaminski J. Domestic dogs: Born human whisperers. Curr Biol. 2021;31: R891–R893. doi:10.1016/J.CUB.2021.05.063
80. Siniscalchi M, D'Ingeo S, Minunno M, Quaranta A. Communication in Dogs. Animals. MDPI AG; 2018. p. 131. doi:10.3390/ani8080131
81. Long RA, Donovan TM, Mackay P, Zielinski WJ, Buzas JS. Effectiveness of Scat Detection Dogs for Detecting Forest Carnivores. J Wildl Manage. 2007;71: 2007–2017. doi:10.2193/2006-230

82. Jamieson LTJ, Baxter GS, Murray PJ. Identifying suitable detection dogs. Applied Animal Behaviour Science. Elsevier B.V.; 2017. pp. 1–7. doi:10.1016/j.applanim.2017.06.010
83. Grimm-Seyfarth A, Harms W, Berger A. Detection dogs in nature conservation: A database on their world-wide deployment with a review on breeds used and their performance compared to other methods. Methods in Ecology and Evolution. British Ecological Society; 2021. pp. 568–579. doi:10.1111/2041-210X.13560
84. Dunn M, Degenhardt L. The use of drug detection dogs in Sydney, Australia. Drug Alcohol Rev. 2009;28: 658–662. doi:10.1111/j.1465-3362.2009.00065.x
85. Guest C, Otto CM. Editorial: Canine Olfactory Detection. Frontiers in Veterinary Science. Frontiers Media S.A.; 2020. p. 100. doi:10.3389/fvets.2020.00100
86. Berns GS, Brooks AM, Spivak M. Scent of the familiar: An fMRI study of canine brain responses to familiar and unfamiliar human and dog odors. Behav Processes. 2015;110: 37–46. doi:10.1016/J.BEPROC.2014.02.011
87. Prichard A, Chhibber R, Athanassiades K, Spivak M, Berns GS. Fast neural learning in dogs: A multimodal sensory fMRI study. Sci Rep. 2018;8: 14614. doi:10.1038/s41598-018-32990-2
88. Jia H, Pustovyy OM, Wang Y, Waggoner P, Beyers RJ, Schumacher J, et al. Enhancement of Odor-Induced Activity in the Canine Brain by Zinc Nanoparticles: A Functional MRI Study in Fully Unrestrained Conscious Dogs. Chem Senses. 2016;41: 53–67. doi:10.1093/chemse/bjv054
89. Jia H, Pustovyy OM, Waggoner P, Beyers RJ, Schumacher J, Wildey C, et al. Functional MRI of the Olfactory System in Conscious Dogs. Dhenain M, editor. PLoS One. 2014;9: e86362. doi:10.1371/journal.pone.0086362
90. Ramaihgari B, Pustovyy OM, Waggoner P, Beyers RJ, Wildey C, Morrison E, et al. Zinc nanoparticles enhance brain connectivity in the canine olfactory network: Evidence from an fMRI study in unrestrained awake dogs. Front Vet Sci. 2018;5: 127. doi:10.3389/fvets.2018.00127
91. Bräuer J, Blasi D. Dogs display owner-specific expectations based on olfaction. Sci Reports 2021 111. 2021;11: 1–10. doi:10.1038/s41598-021-82952-4
92. Peirce JW. PsychoPy-Psychophysics software in Python. J Neurosci Methods. 2007;162: 8–13. doi:10.1016/j.jneumeth.2006.11.017
93. Wagner IC, van Buuren M, Bovy L, Fernández G. Parallel engagement of regions associated with encoding and later retrieval forms durable memories. J Neurosci. 2016;36: 7985–7995. doi:10.1523/JNEUROSCI.0830-16.2016
94. R Core Team. R: A Language and Environment for Statistical Computing. Vienna, Austria: R Foundation for Statistical Computing; 2020. Available: https://www.r-project.org/
95. Yushkevich PA, Piven J, Hazlett HC, Smith RG, Ho S, Gee JC, et al. User-guided 3D active contour segmentation of anatomical structures: Significantly improved efficiency and reliability. Neuroimage. 2006;31: 1116–1128. doi:10.1016/J.NEUROIMAGE.2006.01.015
96. Power JD, Barnes KA, Snyder AZ, Schlaggar BL, Petersen SE. Spurious but systematic correlations in functional connectivity MRI networks arise from subject motion. Neuroimage. 2012;59: 2142–2154. doi:10.1016/J.NEUROIMAGE.2011.10.018
97. Power JD, Mitra A, Laumann TO, Snyder AZ, Schlaggar BL, Petersen SE. Methods to detect,

characterize, and remove motion artifact in resting state fMRI. Neuroimage. 2014;84: 320–341. doi:10.1016/j.neuroimage.2013.08.048

98. Mumford JA, Turner BO, Ashby FG, Poldrack RA. Deconvolving BOLD activation in event-related designs for multivoxel pattern classification analyses. Neuroimage. 2012;59: 2636–2643. doi:10.1016/j.neuroimage.2011.08.076

99. Kriegeskorte N, Goebel R, Bandettini P. Information-based functional brain mapping. Proc Natl Acad Sci U S A. 2006;103: 3863–3868. doi:10.1073/pnas.0600244103

100. Nichols TE, Holmes AP. Non-parametric procedures. Statistical Parametric Mapping: The analysis of Functional Brain Images. Amsterdam: Elsevier; 2007. pp. 253–272.

101. Wickham H. ggplot2: Elegant Graphics for Data Analysis. Springer-Verlag New York; 2016. Available: https://ggplot2.tidyverse.org

102. Allen M, Poggiali D, Whitaker K, Marshall TR, Kievit RA. Raincloud plots: A multi-platform tool for robust data visualization [version 1; peer review: 2 approved]. Wellcome Open Res. 2019;4. doi:10.12688/wellcomeopenres.15191.1

9 Supporting information

9.1 Stimulus material: luminance and spatial extent

Luminance was set to 100 for all images and background, grid-scrambled images were created based on images equally drawn from each category to control for potential low-level visual differences. Face and body images vary in spatial extent (= ratio image / background) due to their shape (mean values: faces = 58.53; bodies = 29.42; $t(118) = 21.17$, $p < 0.0001$), matching them in spatial extent would have required resizing the face images to half their size resulting in less ecologically valid images, but we matched dog and human images within the body and face categories (mean values faces: dogs = 58.55; humans = 58.50; $t(58) = 0.03$, $p = 0.98$; means bodies: dogs = 30.97; humans = 27.87; $t(58) = 1.33$, $p = 0.19$). Further, half of the object images were matched in spatial extent to either body (mean values: bodies = 29.42, matched objects = 29.86, $t(73) = -0.17$, $p = 0.86$) or face (mean values: faces = 58.53, matched objects = 57.23, $t(73) = 0.78$, $p = 0.44$) images and scrambled images were created based on images equally drawn from each category.

9.2 Anatomical search spaces

We localized face and body areas in restrained search spaces to also retrieve anatomically more precise information. For the dog participants, we could not build on previous research due to different template spaces or data unavailability and therefore selected all task-responsive gyri as search spaces. We determined them performing a group-level activation comparison entering the visual stimulation contrast (all conditions > implicit visual baseline) from the first task run in a second-level one sample *t*-test. Since the majority of significant clusters expanded across more than one anatomical region, we decided to not only select regions with a significant local maxima (**Table S1**, section “dog participants**”, Fig 1C**) but all gyri with visual responsive voxels. This resulted in six search spaces for potential face or body regions: medial

suprasylvian, caudal suprasylvian, ectomarginal, occipital, marginal and splenial gyrus (**Fig 2A**). For the human participants, we used bilateral fusiform and occipital face area parcels as face area search spaces and bilateral fusiform and extrastriate body area parcels as body area search spaces derived from previous research [56]. Selecting the top-10% voxels resulted in the following functional region of interest (fROI) sizes for each hemisphere: medial suprasylvian gyrus (32 voxels), caudal suprasylvian gyrus (27 voxels), marginal gyrus (35 voxels; for one dog 23 voxels in the left hemisphere due to lower number of active voxels in contrast bodies > inanimate objects), ectomarginal gyrus (31 voxels), splenial gyrus (34 voxels) and occipital gyrus (23 voxels). For the human participants, selecting the top-10% voxels from each of the four parcels [56] resulted in the following fROI sizes: extrastriate body area (each hemisphere: 137 voxels), fusiform body area (left: 53 voxels; right: 102 voxels), occipital face area (left: 21 voxels, except one participant only had 15 active voxels, and another had no active voxels; right: 79 voxels), fusiform face area (left: 216 voxels, right: 241 voxels).

9.3 Supplemental figures

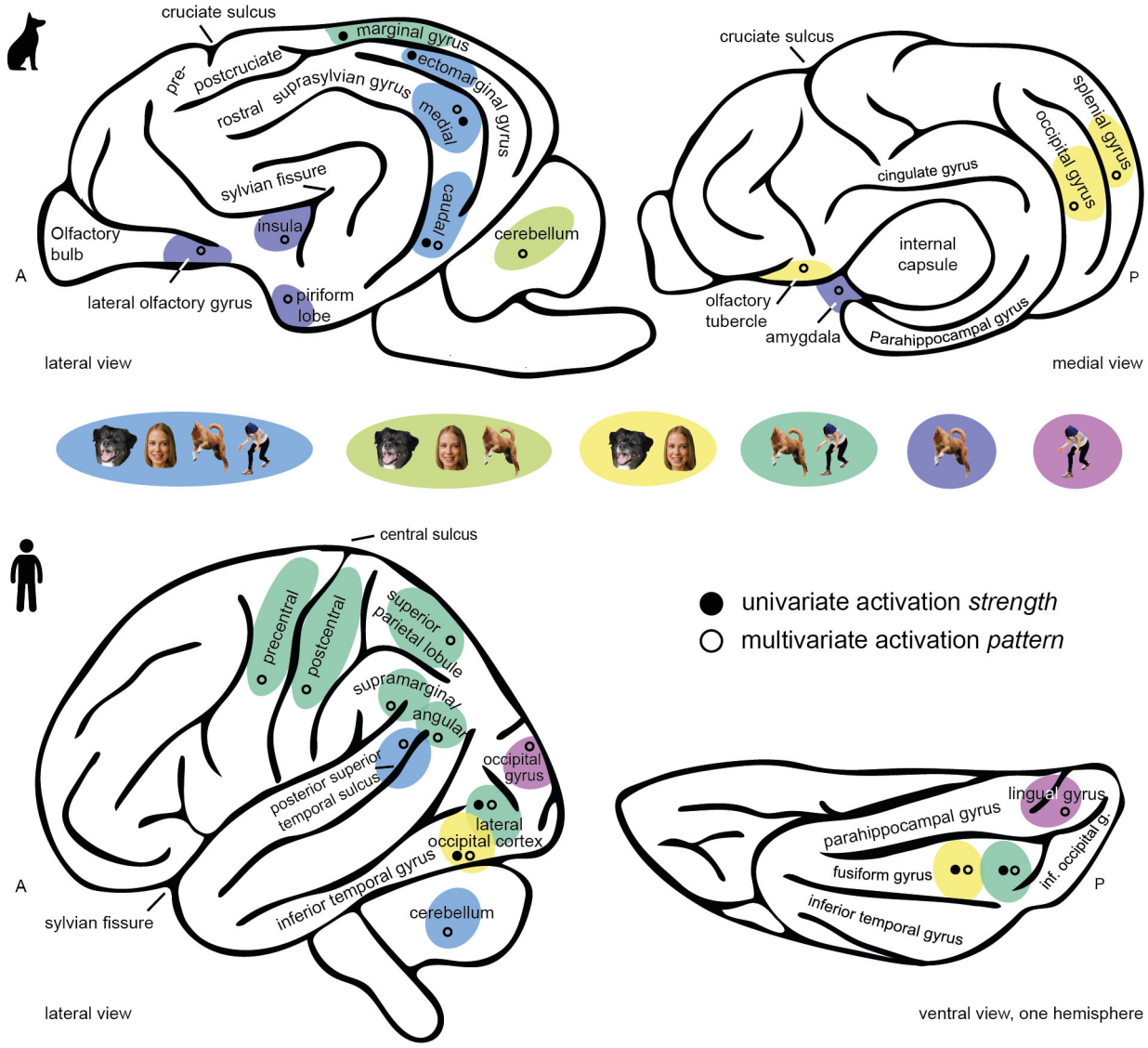

Fig S1. *Summary of the main study findings*. Results from the functional regions of interest (univariate activation strength) and representational similarity analysis (multivariate activation pattern) illustrating the results on schematic brain figures. For simplification, observed results are always summarized on one hemisphere; they do not mark the exact but the approximate anatomical location.

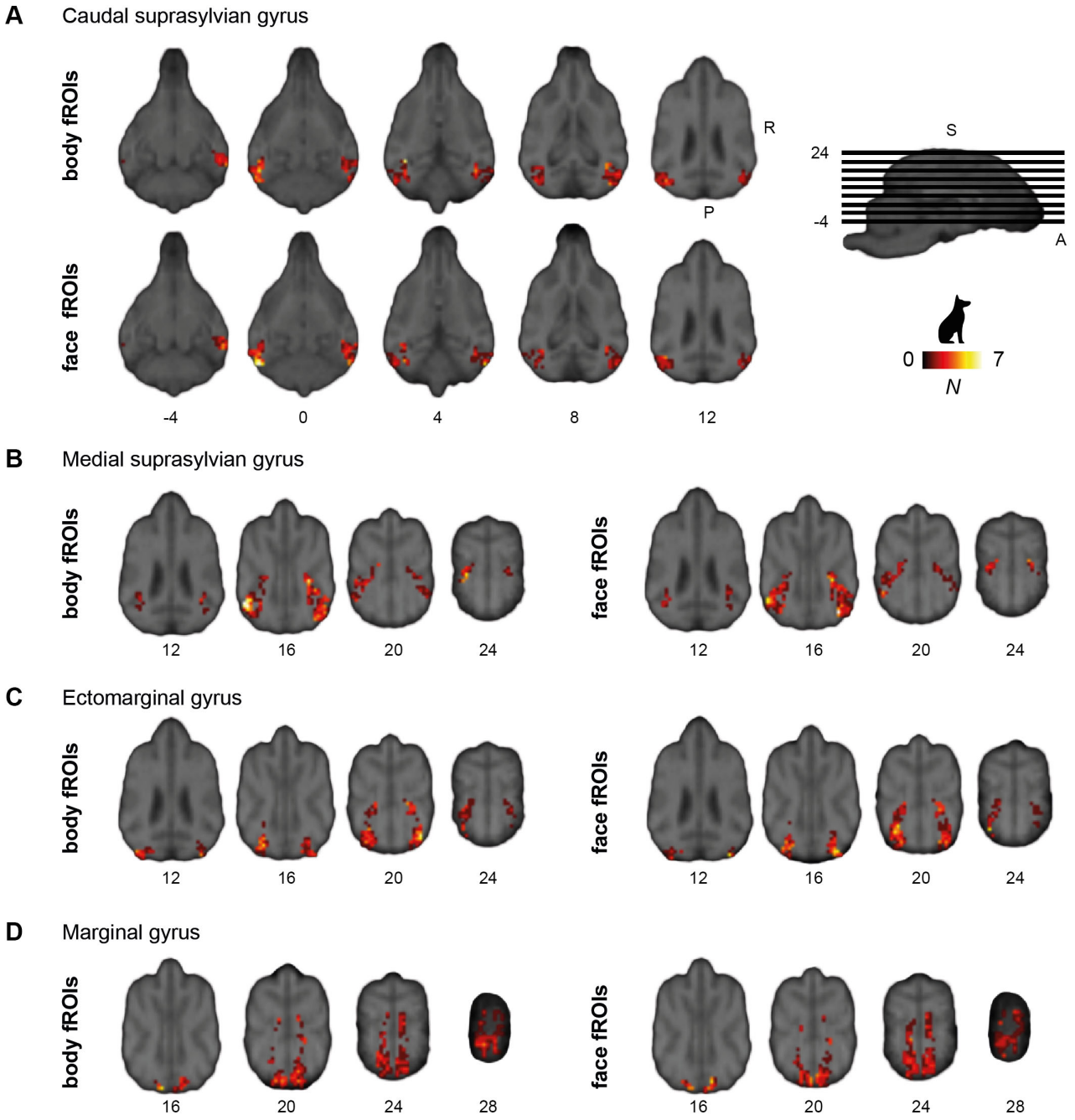

Fig S2. *Overlap of individual functional regions-of-interest (fROIs) from dog participants*. Individual fROIs were defined for faces (> inanimate objects) and bodies (> inanimate objects) within multiple anatomical search spaces (A-D) based on the data from localizer data set (i.e., first task run). The colour of the heat map indicates the amount of overlap between the fROIs of all dog participants. We observed slight individual differences in anatomical location between participants as indicated by a maximum overlap of *N* = 7 from overall 15 participants. The axial plane in panel A (top row) shows the anatomical locations posterior (P) and right hemisphere (R); all axial planes displayed have the same orientation. The sagittal plane displays the cut coordinates (z) and the anatomical locations superior (S) and anterior (A); z-coordinates refer to a canine-breed averaged template [50].

841

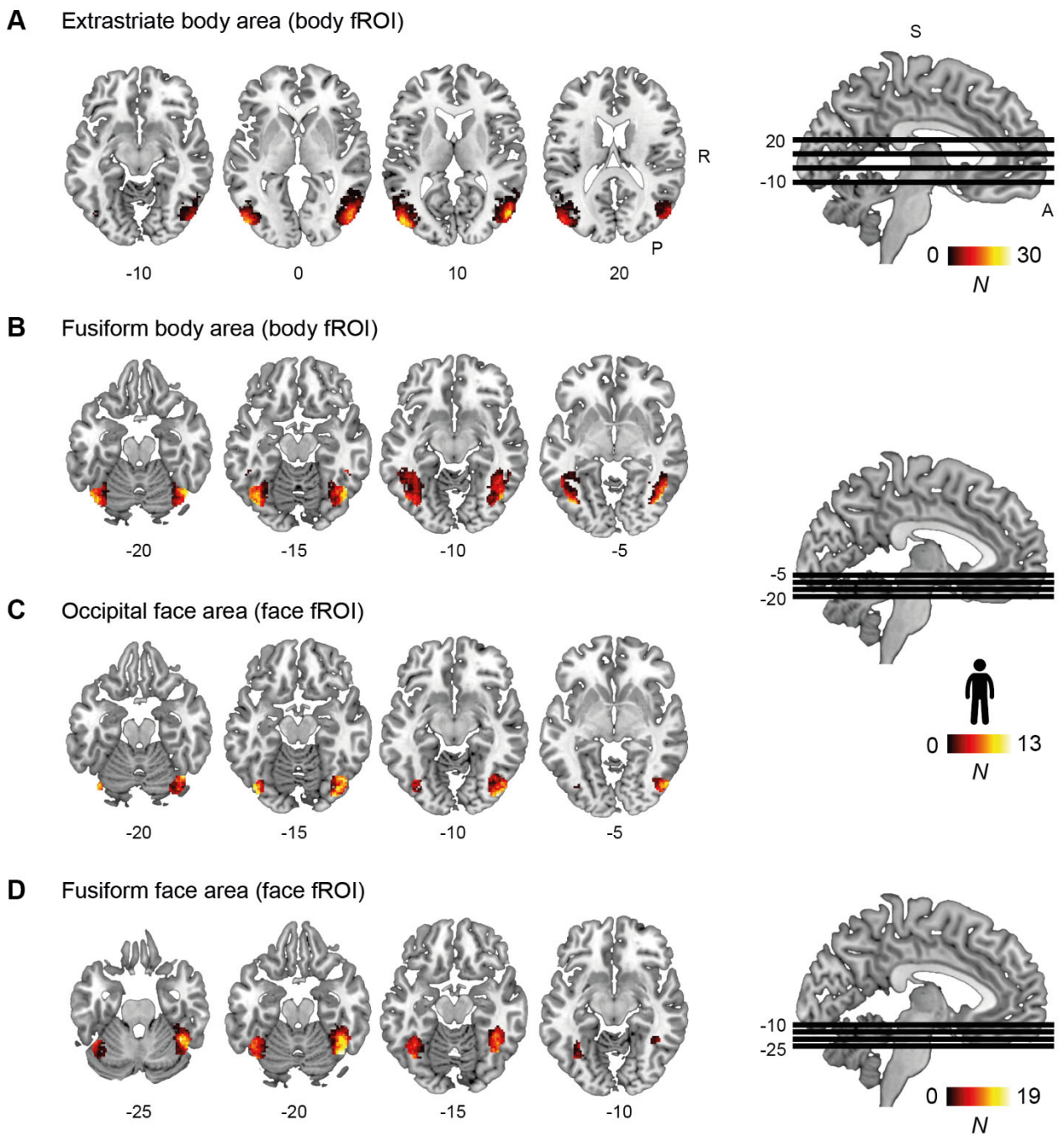

Fig S3. *Overlap of individual functional regions-of-interest (fROIs) from human participants*. Individual fROIs were defined for faces (> inanimate objects) and bodies (> inanimate objects) within multiple anatomical search spaces (A-D) based on the data from the localizer data set (i.e. first task run). The colour of the heat map indicates the amount of overlap between the fROIs of all humans. We observed slight individual differences in anatomical location between participants as indicated by a maximum overlap of *N* = 30 from overall 40 participants. The axial plane in panel A shows the anatomical locations posterior (P) and right hemisphere (R); all axial planes displayed have the same orientation. The sagittal planes display the cut coordinates (z) and the anatomical locations superior (S) and anterior.

9.4 Supplemental tables

Table S1. Task-related activation: localizer data set (task run 1)

Contrast & brain region	Coordinates x	y	z	*z*-value	cluster size
All conditions > implicit visual baseline					
Dog participants					
L medial suprasylvian gyrus	-16	-23	15	4.56	16
L caudal suprasylvian gyrus	-22	-26	-1	4.39	17
L medial suprasylvian gyrus	17	-26	16	4.32	74
L ectomarginal gyrus	-9	-27	21	4.29	52
R ectomarginal gyrus	10	-29	21	4.12	37
R caudal suprasylvian gyrus	22	-24	-1	4.04	24
Human participants					
R middle occipital gyrus	48	-70	-8	Inf	13423
R middle frontal gyrus	20	30	0	Inf	248
L hippocampus	-20	-30	-4	Inf	252
L inferior temporal gyrus	-28	-4	-36	6.89	65
R cerebellum	22	-42	-44	6.80	45

Effects were tested for significance with a cluster defining threshold of p <.001 and a cluster probability threshold of p < 0.05 FWE corrected for multiple comparisons for the dog data and a whole-brain FWE correction for the human data. We report the first local maximum within each cluster for both one sample *t*-tests and for the human data we limit the list to the first five cluster with the highest peak *z*-values. Coordinates for the dog data represent the location of the peak voxels referring to the canine breed-averaged template space[50]; the template along with another dog atlas[51] served to determine anatomical nomenclature for the dog data. Human data coordinates refer to the stereotactic Montreal Neurological Institute (MNI) space we obtained anatomical nomenclature from the Laboratory for Neuro Imaging (LONI) Brain Atlas[52] (LBPA40, http://www.loni.usc.edu/atlases/). Data of both samples is also presented in **Fig 1C**. L, left; R, right.

Table S2. Results from one-way[a] repeated measures analyses of variance (ANOVAs)

Search space (predictor: image category)	df_{Num}	df_{Den}	F	*p*	η^2_g
Dog participants					
Individual body fROIs defined based on bodies > inanimate objects contrast from run 1					
Medial suprasylvian gyrus	2.26	31.68	26.01	**< .0001**	.37
Caudal suprasylvian gyrus	2.26	31.66	12.53	**< .0001**	.25
Ectomarginal gyrus	1.87	26.23	7.48	**.003**	.13
Marginal gyrus	2.36	33.08	8.69	**.001**	.17
Splenial gyrus	2.66	37.19	1.69	.191	.07
Occipital gyrus	2.26	31.58	0.74	.499	.02
Individual face fROIs defined based on faces > inanimate objects contrast from run 1					
Medial suprasylvian gyrus	2.05	28.77	22.13	**< .0001**	.30
Caudal suprasylvian gyrus	2.49	34.90	17.34	**< .0001**	.30
Ectomarginal gyrus	1.75	24.55	12.11	**< .0001**	.18
Marginal gyrus	1.95	27.30	6.38	**.006**	.12
Splenial gyrus	2.34	32.72	1.61	.214	.06
Occipital gyrus	2.26	31.58	0.74	.499	.02
Human participants					
Individual body fROIs defined based on bodies > inanimate objects contrast from run 1					
Extrastriate body area	1.73	67.49	227.01	**< .0001**	.71
Fusiform body area	2.00	77.98	152.22	**< .0001**	.59
Individual face fROIs defined based on faces > inanimate objects contrast from run 1					
Occipital face area	1.98	77.04	175.25	**< .0001**	.64
Fusiform face area	2.12	82.86	187.29	**< .0001**	.63

Note. [a]Dependent variable: *image category* (levels: bodies, faces, inanimate objects, scrambled). *P*-values for group comparison investigating the same research question (i.e., species sensitivity for bodies, species sensitivity for bodies) are Bonferroni-adjusted, resulting in an adjusted *p*-value of 0.008 (= 0.05/6) for the dog body functional regions of interest (fROIs) and face fROIs respectively and an adjusted *p*-value of 0.025 (= 0.05/2) for the human face and body fROIs. *P*-values surviving the adjusted threshold are in bold. Post-hoc comparison results are presented in **Fig 2B**. df_{Num}, degrees of freedom numerator; df_{Den} degrees of freedom denominator; η^2_g, generalized eta-squared.

845

Table S3. Results from 2 × 2[a] repeated measures analyses of variance (ANOVAs)

Search space, predictor	df_{Num}	df_{Den}	F	*p*	η^2_g
Dog participants					
Individual body fROIs defined based on bodies > inanimate objects contrast from run 1					
Medial suprasylvian gyrus					
Species	1	14	3.54	.081	.02
Image category	1	14	7.26	.017	.03
Species × image category	1	14	2.18	.167	.02
Caudal suprasylvian gyrus					
Species	1	14	3.75	.073	.02
Image category	1	14	0.206	.174	.01
Species × image category	1	14	.01	.926	.00
Ectomarginal gyrus					
Species	1	14	2.57	.131	.01
Image category	1	14	1.42	.253	.01
Species × image category	1	14	4.57	.051	.02
Marginal gyrus					
Species	1	14	0.50	.493	.00
Image category	1	14	7.90	.014	.05
Species × image category	1	14	2.25	.156	.03
Splenial gyrus					
Species	1	14	0.03	.859	.00
Image category	1	14	3.71	.074	.03
Species × image category	1	14	1.26	.281	.02
Occipital gyrus					
Species	1	14	1.10	.312	.01
Image category	1	14	0.01	.921	.00
Species × image category	1	14	0.26	.620	.00
Individual face fROIs defined based on faces > inanimate objects contrast from run 1					
Medial suprasylvian gyrus					
Species	1	14	2.51	.135	.01
Image category	1	14	7.11	.018	.03
Species × image category	1	14	1.95	.185	.02
Caudal suprasylvian gyrus					
Species	1	14	1.61	.225	.02
Image category	1	14	10.20	.007	.06
Species × image category	1	14	0.03	.857	.00
Ectomarginal gyrus					
Species	1	14	2.75	.120	.02
Image category	1	14	1.86	.194	.01
Species × image category	1	14	4.22	.059	.03
Marginal gyrus					

Species	1	14	0.08	.786	.00
Image category	1	14	10.03	.007	.07
Species × image category	1	14	1.23	.286	.01
Splenial gyrus					
Species	1	14	0.26	.617	.00
Image category	1	14	1.73	.209	.02
Species × image category	1	14	.70	.416	.01
Occipital gyrus					
Species	1	14	1.21	.289	.02
Image category	1	14	0.03	.855	.00
Species × image category	1	14	3.90	.068	.02
Human participants					
Individual body fROIs defined based on bodies > inanimate objects contrast from run 1					
Extrastriate body area					
Species	1	39	3.15	.084	.01
Image category	1	39	187.26	**< .0001**	.39
Species × image category	1	39	14.15	**.001**	.02
Fusiform body area					
Species	1	39	0.54	.469	.00
Image category	1	39	15.24	**< .0001**	.04
Species × image category	1	39	1.43	.239	.00
Individual face fROIs defined based on faces > inanimate objects contrast from run 1					
Occipital face area					
Species	1	39	0.02	.889	.00
Image category	1	39	36.99	**< .0001**	.07
Species × image category	1	39	1.14	.292	.00
Fusiform face area					
Species	1	39	12.24	**.001**	.02
Image category	1	39	45.23	**< .0001**	.11
Species × image category	1	39	0.28	.600	.00

Note. [a]Dependent variables are *species* (levels: dog, human) and *image category* (levels: bodies, faces). *P*-values for group comparison investigating the same research question (i.e., category selectivity for bodies, category selectivity for faces) are Bonferroni-adjusted, resulting in an adjusted *p*-value of 0.008 (= 0.05/6) for the dog body functional regions of interest (fROIs) and face fROIs respectively and an adjusted *p*-value of 0.025 (= 0.05/2) for the human face and body fROIs. *P*-values surviving the adjusted threshold are in bold, for the dog data none of the *p*-values survived the adjusted threshold. df_{Num}, degrees of freedom numerator; df_{Den} degrees of freedom denominator; η^2_g, generalized eta-squared.

Table S4. Dog data: Pattern similarity during face, body and object perception

	Coordinates (breed-averaged template)				
Contrast & brain region	x	y	z	*t*-value	cluster size
Bodies [dog bodies × human bodies] > inanimate objects					
R caudal suprasylvian gyrus	19	-24	4	5.77	116
Faces [dog faces × human faces] > inanimate objects					
R marginal gyrus	5	-35	21	7.01	245
R olfactory tuberculum	8	8	-2	6.16	80
Conspecific (dog) bodies > heterospecific (human) bodies					
L caudal suprasylvian gyrus	-16	-27	4	5.21	99
L piriform lobe	-15	-3	-4	5.18	95
Animate [dog bodies × human bodies × dog faces × human faces] > inanimate stimuli					
R splenial gyrus	5	-32	7	5.38	70
R caudal suprasylvian gyrus	19	-24	3	5.25	72

Effects were tested for significance with a cluster defining threshold of p <.005 and a cluster probability threshold of p < 0.05 FWE corrected for multiple comparisons. We report the first local maximum within each cluster for all paired sample *t*-tests. The results from the paired sample *t*-tests comparing faces [dog faces × human faces] vs. bodies [dog bodies × human bodies] and conspecific (dog) faces vs. heterospecific (human) faces along with the reversed contrasts [dog bodies × human bodies] < inanimate objects, [dog faces × human faces] < inanimate objects, conspecific (dog) bodies < heterospecific (human) bodies and [dog bodies × human bodies × dog faces × human faces] < inanimate objects did not survive the statistical threshold. Coordinates represent the location of the peak voxels referring to the canine breed-averaged template space[50]; the template along with another dog atlas[51] served to determine anatomical nomenclature for the dog data. Data is also presented in **Fig 3B-D**. L, left; R, right.

Table S5. Human data: Pattern similarity during face, body and object perception

Contrast & brain region	Coordinates (MNI space) x	y	z	*t*-value	cluster size
Bodies [dog bodies × human bodies] > inanimate objects					
R middle occipital gyrus	56	-72	6	14.98	14018
L middle occipital gyrus	-54	-78	10	12.32	1622
L cerebellum	-4	-70	-40	7.33	585
L superior parietal gyrus	-26	-62	68	6.65	1383
R superior frontal gyrus	6	62	-4	6.17	881
L precentral gyrus	-26	-10	50	5.26	570
Bodies [dog bodies × human bodies] < inanimate objects					
L inferior temporal gyrus	-22	-48	-12	11.26	6678
Faces [dog faces × human faces] > inanimate objects					
R fusiform gyrus	46	-42	-20	9.35	1088
Faces [dog faces × human faces] < inanimate objects					
L cerebellum	-20	-54	-18	14.20	7002
R lingual gyrus	24	-56	-8	11.84	5198
L precentral gyrus	-46	6	32	4.77	353
Faces [dog faces × human faces] > bodies [dog bodies × human bodies]					
R lingual gyrus	6	-88	0	11.35	3461
Faces [dog faces × human faces] < bodies [dog bodies × human bodies]					
R middle occipital gyrus	34	-72	10	14.21	39057
R middle orbitofrontal gyrus	24	42	-14	5.53	1087
R cerebellum	8	-72	-38	5.19	572
R cingulate gyrus	2	6	26	4.76	267
Conspecific (human) bodies > heterospecific (dog) bodies					
R fusiform gyrus	44	-44	-22	5.76	1053
L middle occipital gyrus	-54	-72	12	4.87	267
R middle temporal gyrus	40	-54	12	4.81	468
R superior parietal gyrus	16	-54	42	4.60	466
Heterospecific (dog) faces > conspecific (human) faces					
L middle occipital gyrus	-16	-94	6	7.20	8147
Brainstem	6	-40	-26	4.64	618
R middle occipital gyrus	56	-72	0	5.71	349
Animate [dog bodies × human bodies × dog faces × human faces] > inanimate objects					

R middle occipital gyrus	56	-72	0	9.09	2035
L cerebellum	-4	-70	-42	7.30	277
R postcentral gyrus	36	-26	48	5.09	403
R superior parietal gyrus	38	-44	68	4.82	338
R superior frontal gyrus	8	52	-8	4.77	564
Animate [dog bodies × human bodies × dog faces × human faces] < inanimate objects					
L cerebellum	-22	-50	-18	12.63	11878

Effects were tested for significance with a cluster defining threshold of p <.001 and a cluster probability threshold of p < 0.05 FWE corrected for multiple comparisons. We report the first local maximum within each cluster for all paired sample *t*-tests. Results from the reversed contrasts conspecific (human) bodies < heterospecific (dog) bodies and heterospecific (dog) faces < conspecific (human) did not survive the statistical threshold. Coordinates refer to the stereotactic Montreal Neurological Institute (MNI) space and represent the location of the peak voxels. We obtained anatomical nomenclature from the Laboratory for Neuro Imaging (LONI) Brain Atlas [52] (LBPA40, http://www.loni.usc.edu/atlases/). Data is also presented in **Fig 3B-D**.